DIII-D RESEARCH TO PROVIDE SOLUTIONS FOR ITER AND FUSION ENERGY

C.T. Holcomb[1] for the DIII-D Team
Lawrence Livermore National Laboratory
Livermore, California, United States of America
Email: holcomb6@llnl.gov

Abstract

The DIII-D tokamak has elucidated crucial physics and developed projectable solutions for ITER and fusion power plants in the key areas of core performance, boundary heat and particle transport, and integrated scenario operation. New experimental validation of high-fidelity, multi-channel, non-linear gyrokinetic turbulent transport models for the ITER baseline scenario (IBS) provides strong confidence in predicted ITER Q≥10 operation. Experiments in hydrogen identify options for easing H-mode access and give new insight into the isotopic dependence of transport. Analysis of 2,1 islands in unoptimized low-torque IBS demonstration discharges suggests their onset occurs randomly in the constant β phase, often by non-linear 3-wave coupling, thus identifying an NTM seeding mechanism to avoid. At the boundary, measured neutral density and ionization source fluxes are strongly poloidally asymmetric, implying a 2D treatment is needed to model detachment and pedestal fuelling. Deep detachment experiments in ballooning-limited pedestals largely validate predicted trends of pedestal pressure, width and divertor detachment versus pedestal density, using new self-consistent "pedestal-to-divertor" modelling. Measurements of Tungsten (W) sourcing and leakage from a slot divertor with and without ELM control shows ELMs dominate W sourcing and high performance can be maintained without ELMs. Advances have been made in type-1 ELM-free operation in integrated scenarios for ITER and power plants, including negative triangularity. Wide pedestal QH-modes are produced with more ITER-relevant safety factor and shape, and novel feedback-adaptive RMP ELM suppression improves confinement. IBS with W-equivalent radiators can exhibit predator-prey oscillations in T_e and radiation which need control. High-β_P scenarios with q_{min}>2, β_N>4, and H_{98y2}>1.5 are sustained with high density ($\bar{n}$=7E19m^{-3}, f_G~1) for 6 τ_E, improving confidence in steady-state tokamak reactors.

1. INTRODUCTION

The DIII-D tokamak research program utilizes a favourable combination of fusion-relevant size, flexible and varied actuators, and outstanding diagnostics to provide scientific solutions for ITER and fusion pilot plants (FPPs). Program achievements in the last two years discussed in the paper range from focused and detailed physics model validation studies to broad scope integrated operational scenario development, and address processes from the core plasma to divertor surfaces and the main chamber walls. Results fall into three general categories that are the organizational basis for the paper: (1) investigations of requirements for high core plasma performance, including transport, confinement, and stability; (2) boundary heat and particle transport studies, including understanding and optimizing the pedestal, fuelling, divertors, and impurity influx; and (3) integrated operational scenarios for ITER and FPPs, including ELM control solutions, burn control, high-performance steady states, and negative triangularity.

2. REQUIREMENTS FOR HIGH CORE PERFORMANCE

Accurate prediction of ITER's potential fusion performance is needed, and recent DIII-D experiments shed light on transport and stability important for ITER and fusion energy. Extensive high-resolution measurements of kinetic profiles (n_e, T_e, T_i), turbulence fluctuations (low-wavenumber (low-k) n_e and T_e), and impurity transport (Li, C, and Ca) were collected in ITER-similar shaped plasmas designed to examine multi-channel transport in relevant conditions (q_{95}=3.45, low rotation, and ELM-suppressed H-mode). These data showed excellent agreement with machine-learning-assisted nonlinear gyrokinetic CGRYO [1] predictive simulations. [2]. Figure 1 shows the T_i, T_e, n_e, and n_C (carbon) profiles were all reproduced within the scatter of the experimental measurements by the ion-scale nonlinear gyrokinetic simulation that matches experimental heat and particle fluxes, and there is good agreement between predicted and measured low-k density fluctuations. This validation motivated the use of these new techniques to project and optimize performance in ITER conditions. The same modeling framework predicts ITER should achieve the primary goal of Q~10 with ~500 MW of fusion power and suggests paths for further enhancement. Additional simulations predict ITER should still be able to achieve burning plasma conditions with RMP ELM suppression and degraded pedestal conditions.

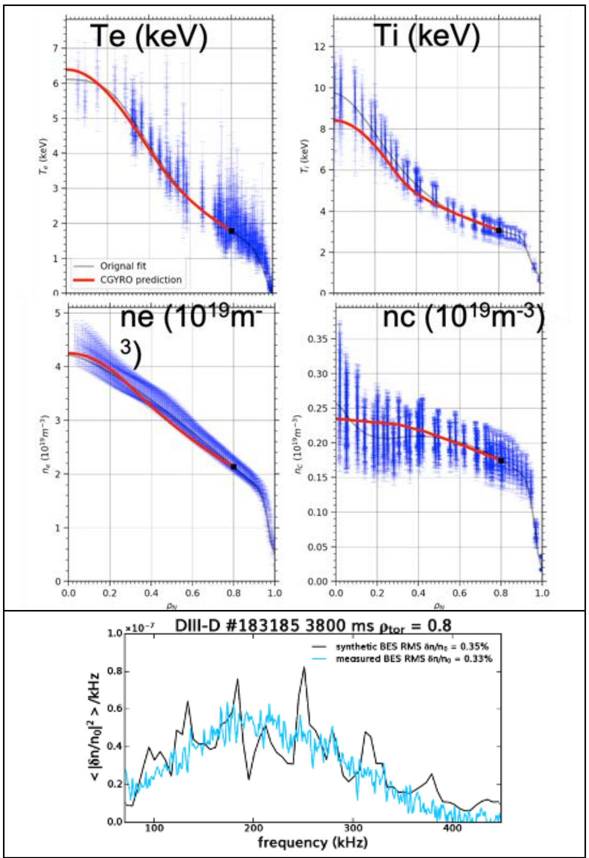

Fig. 1. Gyrokinetic models well reproduce the profiles and turbulence spectrum of ITER relevant plasmas.

Before ITER can achieve Q~10 it must progress through non-nuclear commissioning phases, so DIII-D has developed better solutions for H-mode access in hydrogen and deepened understanding of energy confinement isotope scaling. Experiments in ITER-similar shaped hydrogen plasmas with edge collisionality less than one have demonstrated that the L-H power threshold P_{LH} can be reduced via applied n=3 non-resonant magnetic perturbations (NRMP using the external C-coil [3]. NRMF produces counter-current torque in the plasma edge via Neoclassical Toroidal Viscosity (NTV), driving edge toroidal rotation that increases the local *ExB* shear inside the separatrix, reducing P_{LH} by 25-30%. This reduction is observed for plasmas with balanced neutral beam injection (simulating ITER) as well as for finite NBI torque. MARS-F plasma response calculations for low density ITER hydrogen plasmas predict that significant counter-I_p torque can be generated with optimum phasing of the ITER 3-D coil system just inside the ITER last closed flux surface. P_{LH} is also found to decrease 20-50% by initiating H-mode at lower I_P; the observed hysteresis between L-H and H-L power thresholds in hydrogen suggests ITER could trigger H-mode in the I_P-ramp-up and sustain it into flattop. Impurity seeding has also been shown to reduce P_{LH} using Helium in DIII-D, with up to 15% seeding reducing P_{LH} by 10-20%, and up to 25% seeding reducing P_{LH} by 30-35% (Fig. 2) [3]. Intrinsic carbon impurity dilution also reduces P_{LH} in hydrogen and deuterium plasmas at low edge collisionality compared to "pure" hydrogen plasmas with very low Z_{eff}~1.25 (Fig. 3) [4]. TGLF [5] gyro-fluid and CGYRO gyrokinetic simulations indicate main ion carbon dilution causes an upshift in the ITG critical gradient. In addition, electron non-adiabaticity effects contribute to the higher power threshold in hydrogen, compared to deuterium. The dependence of the ITG critical gradient on ion dilution potentially allows the reduction of P_{LH} during ITER's early operation with hydrogen plasmas via N or Ne light impurity seeding.

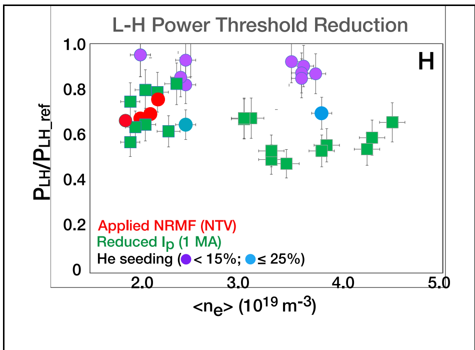

Fig. 2. Reduction in PLH compared to reference case using different techniques.

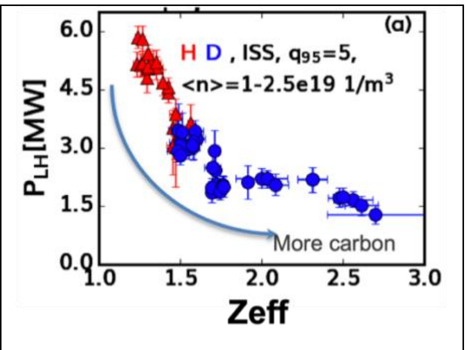

Fig. 3. Intrinsic C-impurity reduces P_{LH}.

New measurements of the detailed turbulence characteristics in dimensionally similar hydrogen and deuterium plasmas partially explain the significant differences in transport and energy confinement time with isotope mass [6]. Energy confinement τ_E is well known to be higher in deuterium (D) than hydrogen (H); in the specific ITER-shaped ELMing H-mode plasmas heated by NBI and ECH in this study, τ_E of the D plasmas exceeded that in H by a factor of ~1.8. The D and H plasmas had well matched β, safety factor q, and T_e/T_i, while normalized gyroradius ρ* and collisionality ν* varied. The factor of 1.8 implies a τ_E-scaling with mass to the power 0.8, which is much stronger than the $\tau_{98,y2}$ mass scaling to the power of 0.19. In contrast, Beam Emission Spectroscopy (BES) measurements of low wavenumber ($k_\perp\rho_i$ < 1) turbulent density fluctuations show the amplitude is higher in D than H, with similar spectral structure, in the radial range 0.35<ρ<0.8. While this is consistent with gyroBohm predictions of normalized fluctuation amplitude scaling as ρ* ~ square root of mass [7], it is apparently at odds with the observed higher τ_E with mass. However, the BES measurements show H has significantly higher radial correlation length than D, ~3.8 cm compared to ~2.4 cm (Fig. 4). This contradicts the gyroBohm prediction that the correlation length should also scale as ρ*, and it offers a potential explanation for enhanced transport and reduced confinement with lower ion mass because random walk diffusivity scales as the square of the correlation length. BES measurements also show H but not D has a low-to-intermediate wavenumber mode with longer poloidal correlation length but lower amplitude (Fig. 4d). These transport physics insights will help validate nonlinear simulations and confinement projections of D-T plasmas in ITER and other future devices.

MHD stability and disruption avoidance is a fundamental requirement for ITER and all tokamak-based power plants. Analysis of m/n=2/1 tearing mode onset time distributions relative to the start time of constant β_N in a wide range of discharge classes indicates most such modes are subject to temporally random processes. A particular focus is DIII-D demonstration low-torque ITER Baseline Scenario (IBS) discharges. Scenario control sequences that reliably and systematically favor either stable or unstable 2/1 operation for the duration of the I_P flattop exist [8]. The stable sequence includes delayed heating and gas flow to regularize ELMs, resulting in a different current profile at the start of the β_N=1.8 phase that modeling predicts is farther from ideal kink and classical tearing limits. For IBS discharges that develop a 2/1 mode, the unstable database onset time distribution in the β_N flattop is well fit by an exponential, meaning 2/1 mode onsets follow Poisson point-process statistics and have a constant onset rate $\lambda=-(dN/dt)/N$, where N is the number of surviving discharges up to time t. (Fig. 5) [9]. Such an onset time distribution is inconsistent with the modes being triggered by purely classical effects the same way in all discharges, i.e., classical stability index Δ' evolving above a critical value in ~1 resistive diffusion time, because modeling predicts this would result in λ peaking at some time, which isn't observed. Poisson statistics imply seeding is happening at random times, and this is consistent with the observation of 3-wave coupling [10] in a majority of 2/1-unstable IBS discharges, whereby 2/1's are triggered by sawtooth precursors coupling to 3/2 islands when differential rotation between rational surfaces approaches zero. Rotation flattening occurs with temporally uniform probability due to n>1 activity. This shows the importance of properly controlling multiple quantities to help avoid 2/1 modes in ITER.

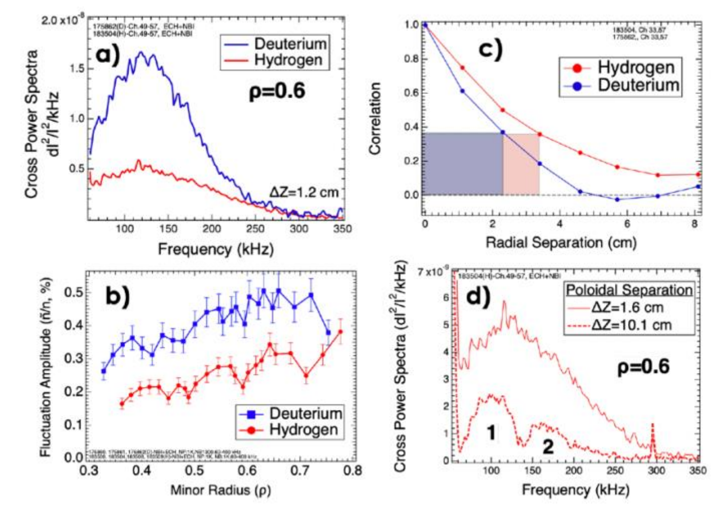

Fig. 4. BES measurements: (a) density fluctuation spectra, (b) fluctuation amplitude profile, (c) radial correlation length, and (d) poloidally separated spectra for hydrogen only showing secondary mode.

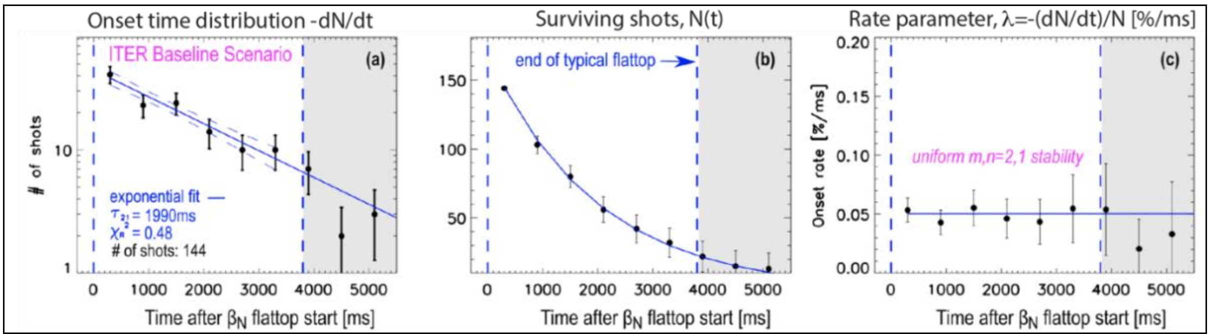

Fig, 5. 2,1 mode onset distribution analysis for unstable ITER Baseline Scenario demonstration discharges.

In experiments with ~10 keV thermal ions minor disruptions are triggered by multi-scale chirping modes associated with the q=1 surface when T_i exceeds a threshold, which is well below the predicted ideal β_N limit [11]. Analysis of magnetic and density fluctuation spectra indicates a strong nonlinear interaction between medium-k and low-k waves. Linear analysis with CGYRO suggest the medium-k modes (cyan ellipse in Fig. 6a) are kinetic ballooning/electromagnetic Alfven ITG modes resonating with thermal ions on passing orbits. MARS-K [12] suggests the lowest-k mode (green ellipse in Fig. 6b) has a mix of kink and tearing eigenstructure, resonating with thermal ions on trapped orbits [13]. This initially local structure can expand from local to global in ~0.5 ms (faster than NTM growth) causing edge islands, current profile redistribution, a moderate drop in I_P, a substantial density spike, impurity influx, and loss of edge temperature. These results confirm that mode resonances with hot thermal tail ions in reactors will be important, and further study is needed to assess mitigations.

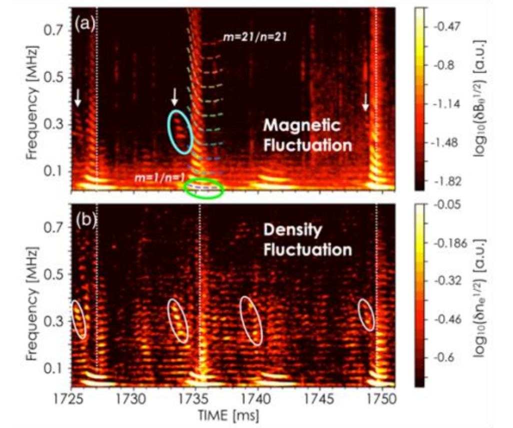

Fig. 6. Fluctuation spectra for hot-ion-driven multiscale chirping modes.

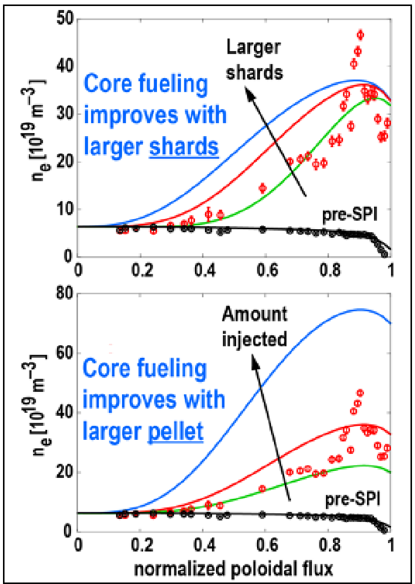

Fig. 7. INDEX modeling (curves) compared to density measurements (points).

Experiments deploying shattered pellet injection (SPI) inform new optimizations of this technique for disruption mitigation on ITER. Previous studies indicated that mixed or staggered low- and high-Z injection may be required to effectively mitigate thermal loads and runaway electrons [14]. New experiments tested the staggered approach with spatially and temporally resolved density and temperature profiles after pure D_2 injection, and mixed Ne/D_2 injection. [15]. This used upgrades to the Thomson scattering diagnostic to enable measurements at ~1 eV (new narrow-band polychromators), asynchronous triggering by pellet ablation light, and "burst mode" close sequential firing of the lasers to capture fast dynamics. A single shattered pellet injector on the low field side close to the Thomson scattering measurements was used. Pure D_2 SPI produces a favorable ten or more millisecond delay to the disruption, but very limited core fueling is observed before the disruption. Even during and after the disruption, when strong mixing of the injected material with the plasma is expected, the edge density significantly exceeds the core density. 1D INDEX [16] transport modeling suggests the poor assimilation is caused by strong outward ∇B induced drift of the ablation cloud and predicts larger pellet shards and sizes will improve D_2 assimilation (Fig. 7) whereas greater speed is less effective because it usually results in smaller fragments. The mixed (~50:50) Ne/D_2 pellet impacts are dominated by Ne; these cause fast radiative collapse of the plasma in a few milliseconds and almost uniform density profile once Ne mixes during and after the thermal quench.

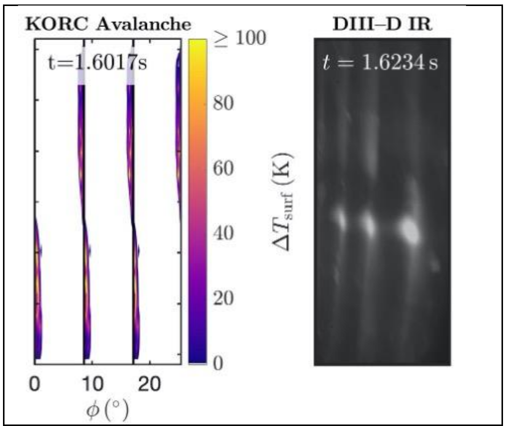

Fig. 8. KORC modelling of inner wall tile edge heating by energetic electrons matches only with inclusion of subcritical electrons.

New comparison of DIII-D infrared imaging measurements of the inner wall to Kinetic Orbit Runaway Electrons Code (KORC) modelling indicates that subcritical energetic electrons (SEEs) produced by the runaway electron (RE) avalanche source at energies below the runaway threshold energy are the primary contributor to transient surface heating of plasma-facing components (PFCs) during final loss events of RE mitigation [17]. The KORC simulations use an analytical first wall for modeling a non-axisymmetric first wall composed of individual tiles; a method was added to approximately include gyrophase to guiding center orbits intersecting PFCs to enable accurate calculations of angle of incidence needed to determine volumetric energy deposition. Simulations show initial REs with significant energy drifts remain confined, even when passing, in magnetic configurations connected to the first wall during the final loss event. But SEEs born at lower energies, below the runaway threshold energy, with little energy drift can be rapidly lost to the first wall (Fig. 8). Qualitative agreement between simulations and infrared imaging is obtained only when SEEs are included. Since typical predictions of PFC heating due to REs only consider high-energy REs, these results provide an important new guideline.

3. BOUNDARY HEAT AND PARTICLE TRANSPORT

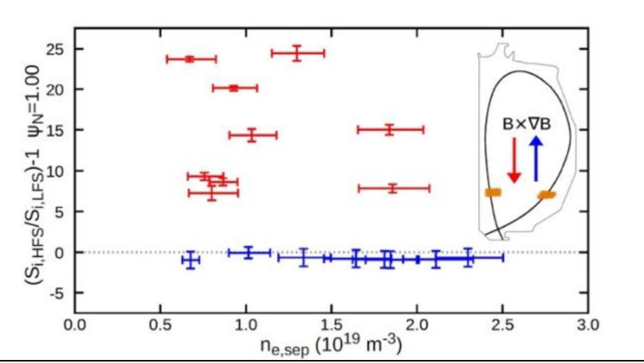

Fig. 9 Ratio of measured neutral ionization source rates on high field side to low field side, minus 1, versus separatrix density.

Studies using DIII-D have elucidated important physics and developed new controls related to the plasma edge and first wall. Novel Lyman-alpha diagnostic measurements [18] show a significant poloidal variation of the main chamber edge ionization source. A one order of magnitude HFS-LFS fueling asymmetry exists when operating with ion Bx∇B drift towards the X-point. Operating with ion B×∇B drift out of the divertor eliminates the imbalance (Fig. 9) [19]. The ionization source asymmetries are related to asymmetric recycling fluxes at the inner and outer divertor targets due to directional parallel plasma flows in the scrape-off layer. Gyrokinetic-plasma and kinetic-neutral simulations using the XGC suite of total-f particle-in-cell codes [20] and DEGAS2 Monte Carlo neutral transport calculations [21] reproduce these observations [22]. The parallel plasma flow in the scrape-off-layer is driven primarily by particle orbit and collisional physics, while turbulent transport across the separatrix determines the overall magnitude. That is, while neutral fueling asymmetries appear in 'neoclassical' simulations that exclude turbulence, quantitative agreement between simulations and experiment is only found when the turbulent particle losses are included. Analysis of these simulations indicate that a low-recycling edge plasma results in novel flow patterns, which cause neutrals to be dominantly produced on one or the other divertor plates. In a highly collisional scrape-off layer as expected in burning plasma devices with larger spatial scale and higher connection length a symmetrization of the parallel plasma fluxes is expected and, therefore, recycling fluxes and main chamber ionization source are expected to become HFS-LFS symmetric. Still, these results motivate 2D modeling to understand fueling in present devices.

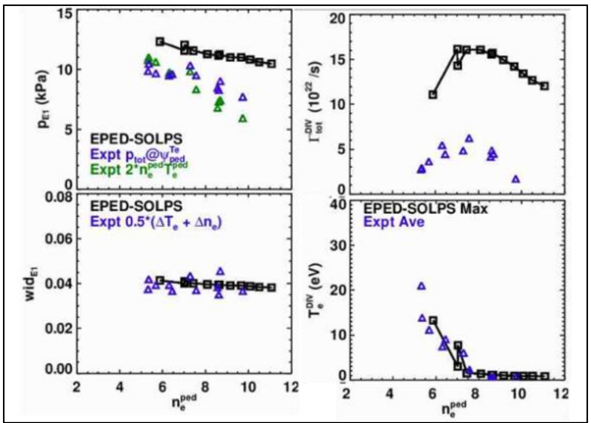

Fig. 10. Measurement and predictive EPED-SOLPS modeling of pedestal pressure and width, divertor ion flux and electron temperature.

DIII-D experimental validation of a new integrated model of the pedestal-to-divertor system enables prediction of pedestal pressures and heat flux widths in future devices. The combined EPED-SOLPS modeling framework was used to predict DIII-D pedestal pressure and width, ion flux to the divertor, and the electron temperature at the divertor target over a range of pedestal density as the divertor was pushed into detachment (Fig. 10) [23]. Measurements of these quantities match the predicted trends with increasing density reasonably well. The model predicted pedestal pressure rate of decrease with density is captured, while pedestal width is nearly constant and quantitatively matched. Predicted and measured ion flux to the divertor reach their peak values at the onset of detachment at roughly the same pedestal density, and target temperatures agree quantitatively, indicating the model accurately predicts the detachment onset density. Accounting for both pedestal and SOL physics in the integrated modeling accurately predicts the pedestal pressure is ballooning limited throughout the density scans, consistent with the generally low pressure observed, while standalone EPED [24] calculations erroneously predict a transition from peeling-limited to ballooning-limited at high density. The key improvement is the integrated model uses an empirical relationship between the divertor temperature from SOLPS [25] and the ratio of pedestal to separatrix densities used by EPED. Similar agreement between experiment and modeling was achieved in three different divertor closure geometries on DIII-D. Bolstered by this validation, the integrated modeling framework is being used to predict pedestals and peak heat flux in proposed fusion pilot plants.

Prediction of detachment in radiative divertor regimes requires validated models of mixed impurity transport and radiation dependence on density, temperature, and P_{SOL}. New 2D multi-wavelength experimental data has been compared to 2D full-drift-physics modeling in single and mixed impurity plasmas with good agreement found [26]. For model validation, it is essential to match the charge state distributions of impurities, which depend on T_e, to accurately predict radiated power density throughout the divertor region. A set of multiple absolutely calibrated spectroscopic and imaging diagnostics in visible and EUV/VUV spectral regions were combined to determine both carbon (C) and nitrogen (N) multi-charge-state divertor concentrations and radiative power constituents in conditions ranging from attached to fully detached. These were compared to 2D UEDGE [27] fluid simulations with full particle drifts and charge state resolved C and N impurities included. The UEDGE simulations match experimentally resolved 2D divertor Te and reproduced the dominant divertor radiated power sources from VUV resonance transitions of C II – C IV and N II – N V, as well as the relative contributions from C and N to the total divertor radiation (Fig. 11). These results provide confidence in the application of these models to design radiative divertor solutions for future devices.

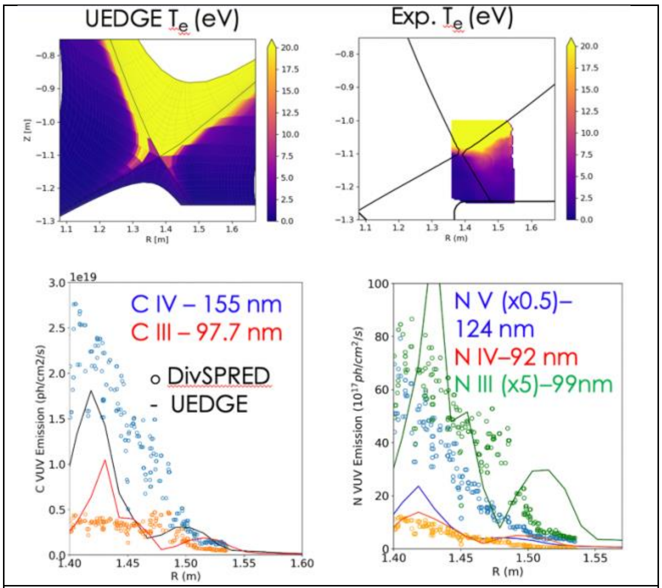

Fig. 11. UEDGE modeling matches measured Te (top) and C and N emission (bottom) in the divertor region.

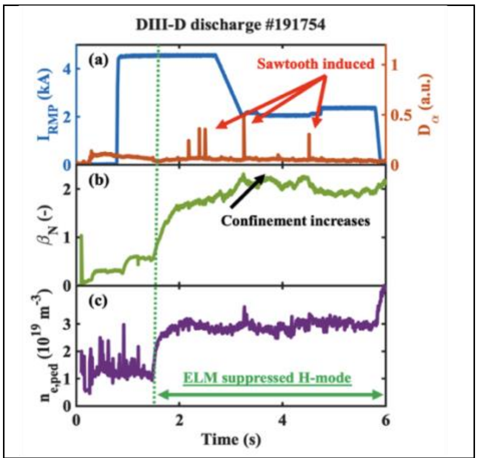

Fig. 12. Feedback adaptive ELM suppression reduces confinement degradation.

A new feedback-adaptive RMP ELM suppression control algorithm was tested on DIII-D that provides a new solution for ELM control in reactors (Fig. 12) [28]. Typically, open loop RMP ELM control with fixed 3D coil currents sufficient for suppressing Type-I ELMs results in degraded pedestal pressure and τ_E. After first achieving ELM suppression with a predetermined coil current I_{RMP}, the new algorithm reduces I_{RMP} while monitoring deuterium-alpha signals for ELMs. In KSTAR, ELM precursor events are detected [29], but so far these have not been seen in DIII-D. Upon detection of a precursor or an ELM, the controller sets a new lower limit for I_{RMP}, increases I_{RMP} to recover suppression, and then attempts to lower it again. Minimization of I_{RMP} increases τ_E in DIII-D test cases by ~18% relative to the start of suppression at full current. The same feedback applied to KSTAR has achieved ~60% τ_E recovery.

Separately, pedestal control and performance has been expanded in two novel regimes [30]. A robust range of counter-Ip edge rotation was found in which density increases with applied n=2 RMP still below the suppression threshold. This is opposite to the well-known density pump out usually observed with RMP that tends to reduce global performance. The greatest line-density increase is about 15% and occurs with a counter-Ip pedestal rotation of ~40 km/s. (Fig. 13). Doppler back scattering measurements show the prompt increase in particle confinement is due to a drop in inter-ELM pedestal turbulence amplitude and a switch from an ion- to electron-mode at the pedestal top. The other new development is the application of counter-Ip ECCD at the pedestal to reduce the required RMP amplitude for ELM suppression. This results in a higher pedestal pressure with the same τ_E and is a useful tool for pedestal physics exploration.

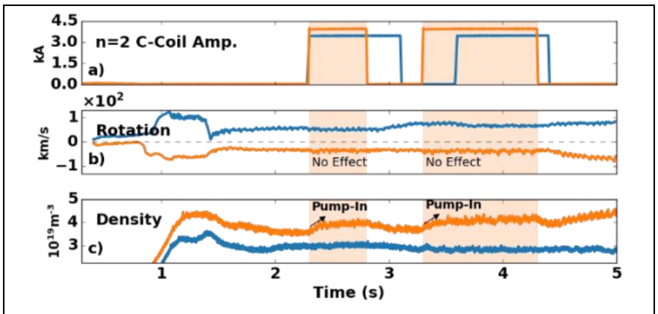

Fig. 13. RMP with edge counter-Ip rotation (orange) raises particle confinement.

Other experiments have evaluated the impacts of ELM control on H-mode plasmas with q_{95}=3.75 and an outer strike point in a Tungsten (W) coated small angle slot divertor not connected to a cryopump [31], [32]. Without any ELM control, ELMs dominate the W source that contaminates the core plasma. The ELMs, and therefore the W source, tend to be larger with greater plasma stored energy W_{MHD} and lower pedestal collisionality ν^*_{ped}. ELM mitigation and in some cases full suppression (Fig. 14) with n=3 RMPs significantly reduce or eliminate the W source per ELM at high W_{MHD} and low ν^*_{ped} (Fig. 15). Higher W_{MHD} and lower ν^*_{ped} are observed to be approximately constant for the duration of the ELM suppressed phase in the I_P flattop (~1.5 seconds), indicating that W transport out of the core is still sufficiently high to avoid W build-up despite loss of ELMs, which are also known to flush impurities. These results suggest RMP ELM suppression integrated with a W slot divertor is a solution capable of maintaining high fusion performance with minimal PFC damage in future reactors.

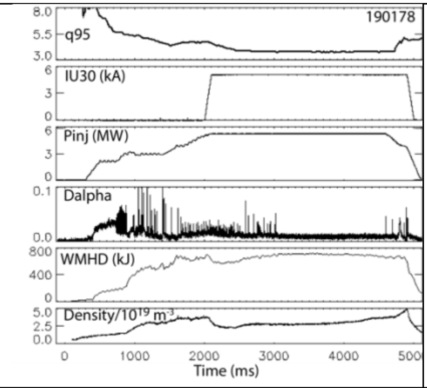

Fig. 14. N=3 RMP ELM suppression with outer strike point in W-coated small angle slot divertor.

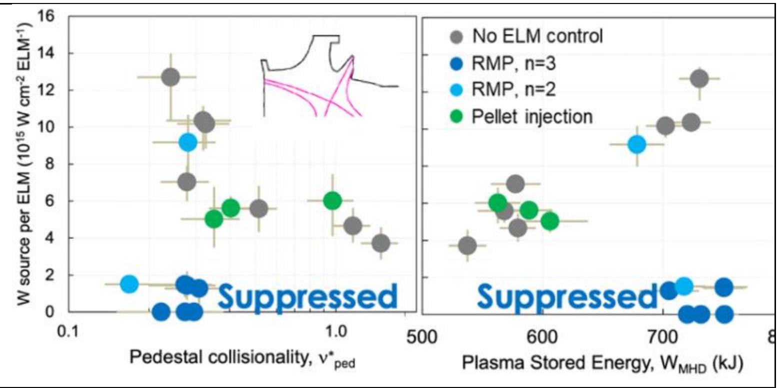

Fig. 15. Measured Tungsten source per ELM versus pedestal collisionality and plasma stored energy. Inset shows the upper divertor geometry with an OSP in a W-coated small angle slot. Legend indicates ELM control method.

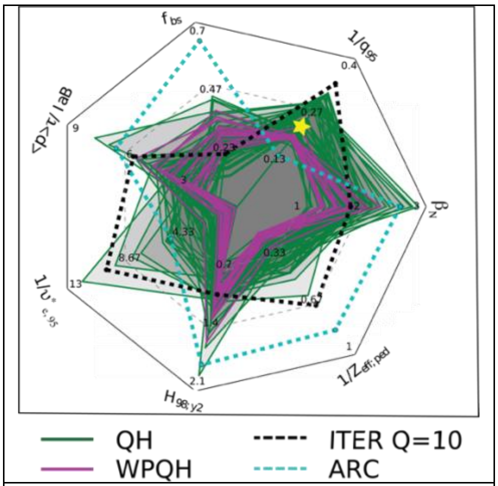

Fig. 16. Spider plot showing key metrics for IBS (Q=10), ARC reactor [39], and achieved DIII-D QH- and WPQH-mode discharges.

4. INTEGRATED OPERATIONAL SCENARIOS

A high-level program goal is to put core and edge solutions together for sustained high performance with sufficient heat and particle exhaust and without damaging transients like ELMs. Several paths are being pursued to provide such operational scenarios for ITER and FPPs along with discerning the key physics requirements of each. Significant progress has been made in expanding the operational space and physics understanding of Wide-Pedestal Quiescent H-mode (WPQH-mode) as a promising naturally ELM-stable high-performance scenario for reactors (Fig. 16) [33]. The range of q_{95} of WPQH-mode operating at low torque (<1.5Nm) has recently been reduced to 4.2, which is the lowest yet achieved for this scenario in a quasi-stationary state. Power handling capability has also been increased from 5.5MW to 7.5MW, limited by the available balanced NBI power to keep the net torque small. WPQH at net-zero injected torque has been achieved in both directions of I_P, with both favorable and unfavorable ion Bx∇B drift directions, and in different plasma shapes including the ITER similar shape. WPQH-modes are observed to lack the standard H-mode ion-channel power degradation of τ_E [34]. Extensive transport modeling using TGYRO/TGLF shows that this could be explained by the large Shafranov shift in these plasmas stabilizing core drift-wave instabilities and enabling high-confinement ELM-stable plasmas [35]. A low ExB shear region in the middle of the pedestal is thought to allow the destabilization of broadband MHD and/or turbulence observed there. Detailed analyses and numerical modeling of pedestal instabilities identify one mild peeling-ballooning mode and one drift-Alfven wave that compete to produce the wide pedestal [36]. The divertor heat width λ_q of WPQH-mode plasmas is observed to increase with edge broadband MHD/turbulence with cases where λ_q exceeds the neoclassical Eich scaling [37]. Modeling indicates this is associated with turbulence spreading across the separatrix. [38]

DIII-D tested the impacts of W radiation on the burn phase of the ITER Baseline Scenario (IBS) by using W-equivalent radiators [40]. Kr and Xe mixtures have the same radiative loss rates L_z in the DIII-D core as W in the hotter ITER core, so they are injected as proxies to simulate the impacts of W radiation in ITER. IBS demonstration plasmas were generated with these radiators (Fig. 17) spanning the range of expected impurity

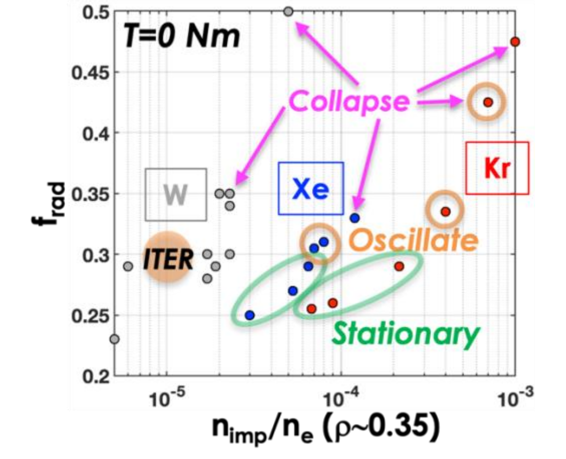

Fig. 17. IBS radiation fraction versus impurity concentration using W-equivalent radiators.

concentration and W radiated fraction with net NBI torque scanned between 0 and 5 Nm. Impurity concentrations of $n_{Kr}/n_e{\sim}2{\times}10^{-4}$ and $n_{Xe}/n_e{\sim}6{\times}10^{-5}$ correspond to ITER expected $n_W/n_e{\sim}$1e-5 and $f_{rad}{\sim}30\%$ (given DIII-D's lower density than ITER). In the range of f_{rad}=0.25-0.35, a bifurcation is observed, which either allows the scenario to be stationary, or trigger an oscillatory regime with T_e and f_{rad} oscillating out of phase, and the core oscillating out of phase from the edge/pedestal. A Lotka-Volterra predator-prey model with full profiles, diffusion, and noise was designed to gain insight into the dynamics of the system, and its results show that this model can reproduce the experimental T_e and f_{rad} profiles. To explore the more specific physics of a tokamak plasma and extrapolate to ITER, a physics-based model not constrained to oscillate was designed that successfully reproduces the oscillatory behavior of the experiment, with the correct range of amplitude and phase difference observed, remaining robustly stable to variations in inputs. This indicates a reasonable understanding of the drivers of this phenomenon for projecting to ITER, as well as mimicking alpha power and burn dynamics in DIII-D, demonstrating the relevance of carbon-wall machines for fusion energy physics. Future DIII-D experiments will aim at controlling burn phase oscillations.

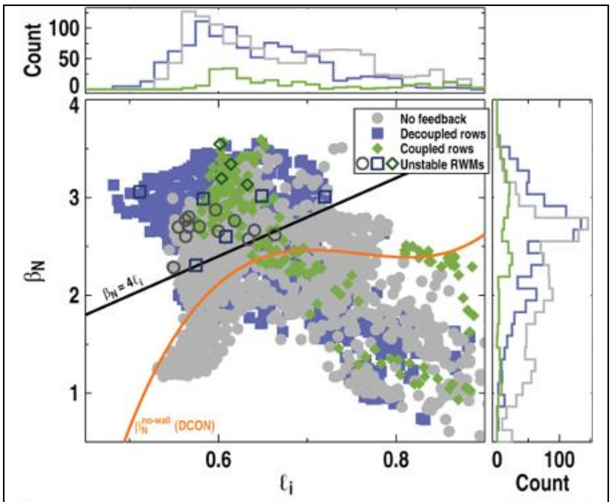

Fig. 18. In the High-β_P Scenario, RWM control using decoupled coil rows extends stable operation.

The High-β_P Scenario for steady-state operation with high fusion gain and high bootstrap current fraction (f_{BS}) has been optimized for improved MHD stability. One advance is the use of a novel variable-poloidal-spectrum mode control with internal non-axisymmetic coils (I-coils) [41]. A high-β_P regime is often investigated on DIII-D using slow continued ramps of I_P and/or B_T throughout the discharge, resulting in varying q_{95}. The new feedback scheme configures the upper and lower I-coil rows in two independent feedback loops, allowing the feedback field poloidal spectrum to vary and track changes in the plasma mode structure over a range of q_{95} from 6 to 11. The q_{95} dependence of the observed phase difference between the coil rows during feedback is qualitatively compatible with ideal MHD simulations of the least-stable plasma kink mode. This feedback facilitated high β_N operation in excess of the ideal MHD n=1 no-wall kink stability limit, with a broad current profile and low internal inductance, β_P=3%, and $f_{BS}{\approx}60\%$. Such performance extensions, particularly to lower internal inductance ℓ_i (Fig. 18), are not obtained using coupled coil rows. Variable-spectrum feedback helps avoid beta collapses caused by marginally stable resistive wall mode (RWM) activity. These results underscore the utility of MHD mode control for accessing high-β fusion-relevant regimes. The variable spectrum feedback approach is a straightforward way to improve resilience to variations in mode structure that occur as plasma parameters change. The extension to lower ℓ_i is expected to improve the coupling of the plasma kink mode to external (i.e., feedback) fields and beneficial wall eddy currents, and is compatible with high-f_{BS} operation.

In a few High-β_P Scenario discharges, further tuning of the ramp-up sequence has resulted in higher performance sustained for longer [42]. $\beta_N{\sim}4.2{\sim}6\ell_i$, $\beta_T{\sim}3.3\%$, and $q_{min}{>}2$ was sustained for ~0.7 of a current profile relaxation time (more than 6 τ_E), with $f_{BS}{\sim}80\%$, a large-radius internal transport barrier, $H_{98y2}{\sim}1.7$, $f_{Gr}{\sim}1$, and stationary impurity levels (Fig. 19). The high-performance phase is terminated by fast growing modes destabilized at the n=1 ideal MHD, ideal-wall kink stability limit, following transient β_N excursions above the feedback-controlled target. Limitations of the β_N feedback control algorithm enable transient excursions above the target. A rapidly growing n=1 mode appears as the limiting instability during one of these excursions, preventing stationary sustainment of high performance. GATO [43] calculations indicate that the plasma is crossing the ideal-wall n=1 kink limit right before the disruption. New microwave and RF capabilities for off-axis current drive (top launch EC [44], helicon [45], high field side lower hybrid [46]) could remove the need for a low-β-phase B_T ramp down and high-β-phase slow I_P ramp up to achieve fully noninductive operation with improved coupling between modes and the wall, thus increasing the ideal-wall β_N limit. Improved β_N feedback controls are being developed to avoid transient excursions. These results improve confidence that the High-β_P Scenario is an attractive option for steady-state operation in ITER and power plants.

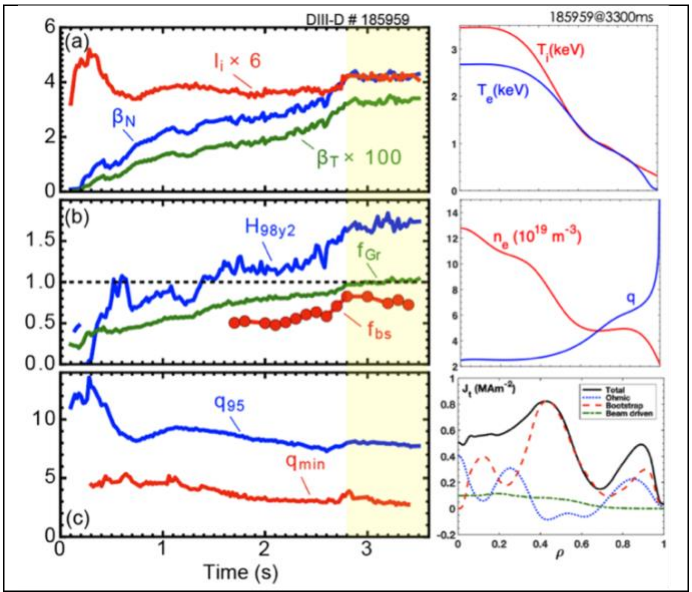

Fig. 19. Time histories and profiles for High-β_P scenario optimized for higher performance.

DIII-D carried out a multiple-week campaign in 2023 to investigate negative triangularity (NT) [47], building upon previous results from TCV [48] and DIII-D [49]. Graphite-tile armor was installed on the low-field-side lower outer wall to obtain high power diverted plasmas with strong NT (Fig. 20a). High confinement ($H_{98y,2}\geq1$), high current ($q_{95}<3$), and high normalized pressure ($\beta_N>2.5$) plasmas were achieved at high-injected-power in a strong NT-shape with a lower outer divertor X-point that also demonstrated high normalized density ($n_e/n_G\leq2$) and a detached divertor without ELMs. The L-H transition was inhibited at δ_{avg} = - 0.5 at all injected beam powers (up to 12 MW) and torques possibly due to restricted second stability access from infinite-*n* ballooning modes predicted in NT [50], [51]. However, while not an H-mode edge, there is a slight T_e pedestal compared to L-mode plasmas, resulting in the so-called NT-edge. A range of discharges were studied from high gain cases with q_{95}=2.7, to cases with q_{95}=4 and 50-60% non-inductive current. Both cases achieved high performance (β_N>2.5 and $H_{98y,2}$~1, Fig. 20b). In NBI-heated plasmas, high central densities up to n_{e0}~$1.4\text{x}10^{20}\text{m}^{-3}$ and high Greenwald fractions f_G approaching 2 were achieved, whereas in plasmas with only Ohmic heating f_G was limited to 1 (Fig. 20c). Divertor detachment was obtained (Fig. 19d) in density ramps with only D_2 injection in both favorable and unfavorable ion B×∇B drift directions [52]. This showed a more gradual L-mode-like detachment evolution with no detachment cliff [53]. These results demonstrate several key principles indicating the potential viability of NT as the basis for a fusion power plant [54].

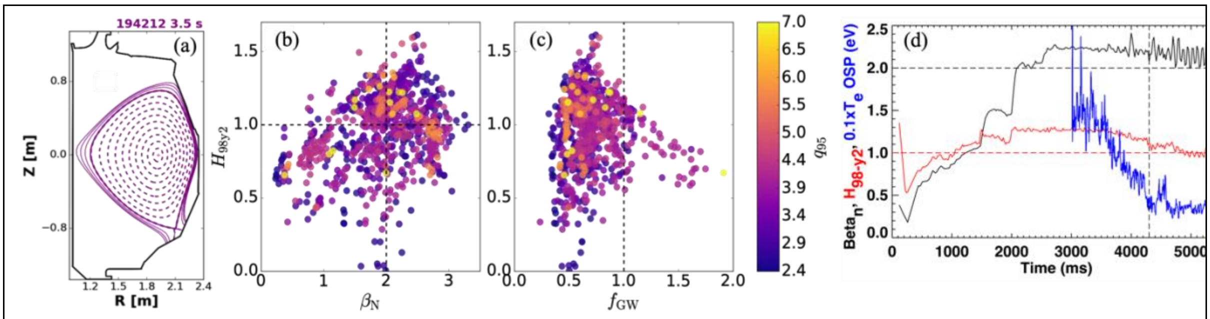

Fig. 20. (a) NT shape with armored tiles. (b) and (c) show H_{98y2}, β_N, and density limit fraction f_G for a range of q_{95} averaged over 400 ms stationary periods. (d) β_N, H_{98y2}, and outer strike point Te in NT detached discharge.

5. FUTURE PLANS AND CONCLUSIONS

The DIII-D program plans several hardware upgrades between now and 2028 that will better enable it to close key knowledge gaps for a successful ITER program and design of fusion pilot plants. These include increases in flexible heating and current drive power in parallel with testing a series of new divertor designs and new technologies. Raising electron cyclotron heating and current drive delivered power from 5 MW in 2024 to 14 MW in 2028 is key for testing ITER and FPP integrated scenario physics with relevant higher Te/Ti, lower torque, lower fast ion fraction, lower collisionality, and higher density in a range of inductive and non-inductive equilibria. New high harmonic fast wave (Helicon) and high-field-side launched Lower Hybrid systems coming online will further enhance DIII-D's ability to achieve and test advanced scenarios with broad current and pressure profiles for high β_N steady-state operation in higher density plasmas. The divertor stages will start with a new relatively small-volume closed divertor optimized for a large volume highly shaped core plasma predicted to enable high peeling-limited pedestal pressures at low collisionality and reactor-relevant pedestal neutral opacity. This will be succeeded by a larger Stage-2 slot-like divertor with sufficient volume for detailed radiative heat dissipation and detachment studies with moderate shaping. Divertor Stage 3 will be optimized to integrate high core performance with efficient and capable heat and particle exhaust. Stage-3 will arrive in 2028 when upgrades to ECH, RF, and NBI systems are complete, providing up to ~43 MW total heating power. Along the way, DIII-D will develop technologies: an ECH gyrotron test socket is planned, along with dedicated vacuum ports to test new reactor-relevant diagnostics and first wall materials. The novel Helicon and High-Field-Side Lower Hybrid systems will be further developed, as well as disruption mitigation systems like shell pellets designed to reach and cool the core from the inside out [55], and a passive 3D coil designed to deconfine and render harmless runaway electrons [56].

In conclusion, DIII-D research is finding solutions for fusion energy. It has provided tools and identified essential requirements for achieving high core fusion performance. These include validated turbulent transport models capable of predicting kinetic profiles, new understanding of the isotopic dependence of turbulence, and the demonstration of methods to ease H-mode access in ITER's non-nuclear phases. Harmful MHD instability causes have been diagnosed and new guidance for instability avoidance and disruption mitigation provided. DIII-D research has elucidated boundary heat dissipation and particle fuelling processes that need to be understood and controlled for successful fusion energy. These include assessments of ionization source asymmetries, validation of a model for pedestal and heat flux behaviours during detachment, and characterization of mixed impurity concentrations needed to dissipate power into the SOL. Also, RMP ELM control was shown to mitigate Tungsten contamination, and feedback controlled RMPs were shown to minimize confinement degradation during suppression. Finally, DIII-D has put a range of integrated operational scenarios on a firmer basis. Naturally ELM-free wide pedestal quiescent H-mode operation has been extended to a larger range of reactor relevant conditions, and ITER Baseline Scenarios have been tested with Tungsten equivalent radiators to study and control stationary- and oscillating-temperature regimes that result. For steady-state operation, the High-β_P Scenario has reached higher β_N with lower ℓ_i using new scenario controls. Negative triangularity has been shown to be capable of high performance with a non-ELMing edge and divertor detachment, offering a novel option for future fusion reactors.

ACKNOWLEDGEMENTS

This material is based upon work supported by the U.S. Department of Energy, Office of Science, Office of Fusion Energy Sciences, using the DIII-D National Fusion Facility, a DOE Office of Science user facility, under Awards DEFC02-04ER54698 and DE-AC52-07NA27344.

DISCLAIMER

REFERENCES

[1] CANDY, J., et al., "A High-Accuracy Eulerian Gyrokinetic Solver for Collisional Plasmas", Journal Comp. Phys. 324, 73 (2016).

[2] HOWARD, N., "Performance and Transport in ITER: Multi-Channel Validation in DIII-D ITER-Like Conditions and Predictions of ITER Burning Plasmas Via Nonlinear Gyrokinetic Profile Prediction", 29th IAEA Fusion Energy Conference (Proc. Int. Conf. London, UK, 2023), IAEA, Vienna (2023)

[3] SCHMITZ, L., "Accessing and Maintaining Robust H-mode in ITER Pre-Fusion Power Operation (PFPO) Plasmas", 29th IAEA Fusion Energy Conference (Proc. Int. Conf. London, UK, 2023), IAEA, Vienna (2023)

[4] CALLAHAN, K., "Origin of the L-H Threshold Isotope Effect in DIII-D Hydrogen and Deuterium Plasmas", 29th IAEA Fusion Energy Conference (Proc. Int. Conf. London, UK, 2023), IAEA, Vienna (2023)

[5] STAEBLER, G., et al., “A Theory-Based Transport Model With Comprehensive Physics”, Phys. Plasmas 14, 055909, (2007).
[6] MCKEE, G., “Turbulence, Transport and Confinement Dependence on Isotope Mass in Dimensionally Similar H-Mode Plasmas on DIII-D”, 29th IAEA Fusion Energy Conference (Proc. Int. Conf. London, UK, 2023), IAEA, Vienna (2023)
[7] MCKEE, G., et al., “Non-dimensional Scaling of Turbulence Characteristics and Turbulent Diffusivity”, Nucl. Fusion, 41, 1235 (2001).
[8] TURCO, F., et al., “Modelling and Experiment to Stabilize the ITER Baseline Scenario in DIII-D”, submitted to Phys. Rev. Lett., 2023.
[9] BARDOCZI, L., “The Root Cause of Disruptive NTMs and Paths to Stabile Operation in DIII-D ITER Baseline Scenario Plasmas”, 29th IAEA Fusion Energy Conference (Proc. Int. Conf. London, UK, 2023), IAEA, Vienna (2023)
[10] BARDOCZI, L. et al., “Neoclassical Tearing Mode Seeding by Nonlinear Three-Wave Interactions in Tokamaks”, Phys. Rev. Lett. 127, 055002 (2021).
[11] DU, X. et al., “Multiscale Chirping Modes Driven by Thermal Ions in a Plasma with Reactor-Relevant Ion Temperature”, Phys. Rev. Lett. 127, 025001 (2021).
[12] LIU, Y. et al., “Toroidal Self-Consistent Modeling of Drift Kinetic Effects on the Resistive Wall Mode”, Phys. Plasmas, 15, 112503 (2008).
[13] LIU, Y. et al., “Modelling of Thermal-Ion-Driven Internal Kink in DIII-D High-Ti Plasmas”, Nucl. Fusion, 62, 086050, (2022).
[14] LEHNEN, M., 2022 Disruptions in ITER URL https://conferences.iaea.org/event/281/contributions/24711/
[15] LVOVSKIY, A. et al., “Density and Temperature Profiles After Low-Z and High-Z Shattered Pellet Injections on DIII-D”, submitted to Nucl. Fusion, 2023.
[16] MATSUYAMA, A. et al., “Transport Simulations of Pre-Thermal Quench Shattered Pellet Injection in ITER: Code Verification and Assessment of Key Trends”, Plasma Phys. Controlled Fusion, 64, 105018 (2022).
[17] BEIDLER, M., “Wall Heating by Subcritical Energetic Electrons Generated by the Runaway Electron Avalanche Source”, 29th IAEA Fusion Energy Conference (Proc. Int. Conf. London, UK, 2023), IAEA, Vienna (2023)
[18] ROSENTHAL, A., et al., “A 1D Lyman-Alpha Profile Camera for Plasma Edge Neutral Studies on the DIII-D Tokamak”, Rev. Sci. Instrum. 92, 033523 (2021).
[19] LAGGNER, F., “Disentangling H-Mode Pedestal Structure and Neutral Ionization Source”, 29th IAEA Fusion Energy Conference (Proc. Int. Conf. London, UK, 2023), IAEA, Vienna (2023)
[20] KU, S.-H., et al., “A Fast Low-to-High Confinement Mode Bifurcation Dynamics in the Boundary-Plasma Gyrokinetic Code XGC1”, Phys. Plasmas, 25, 056107 (2018).
[21] STOTLER, D. et al., “Neutral Gas Transport Modeling With DEGAS 2”, Contrib. to Plasma Phys. 24, 392 (1994).
[22] WILKIE, G., “Kinetic Simulations of Pedestal Fuelling Asymmetry and Implication for Scrape-Off Layer Flows”, 29th IAEA Fusion Energy Conference (Proc. Int. Conf. London, UK, 2023), IAEA, Vienna (2023)
[23] SNYDER, P., “Self-Consistent Integrated Modeling of the Pedestal, Scrape-Off Layer, and Divertor”, 29th IAEA Fusion Energy Conference (Proc. Int. Conf. London, UK, 2023), IAEA, Vienna (2023)
[24] SNYDER, P. et al., “A First-Principles Predictive Model of the Pedestal Height and Width: Development, Testing, and ITER Optimization With the EPED Model”, Nucl. Fusion, 51, 103016 (2011).
[25] WIESEN, S. et al., “The New SOLPS-ITER Code Package”, J. Nuclear Materials, 463, 480, (2015).
[26] SCOTTI, F., “2D Characterization of Radiative Divertor Regimes With Impurity Seeding in DIII-D H-Mode Discharges”, 29th IAEA Fusion Energy Conference (Proc. Int. Conf. London, UK, 2023), IAEA, Vienna (2023)
[27] ROGNLIEN, T. et al., “A Fully Implicit, Time Dependent 2-D Fluid Code for Modeling Tokamak Edge Plasmas”, J. Nucl. Mater. 196, 347, (1992).
[28] SHOUSHA, R., “Closed Loop RMP ELM Suppression With Minimized Confinement Degradation Using Adaptive Control Demonstrated in DIII-D and KSTAR”, 29th IAEA Fusion Energy Conference (Proc. Int. Conf. London, UK, 2023), IAEA, Vienna (2023)
[29] KIM, S., et al., “Optimization of 3D Controlled ELM-Free State With Recovered Global Confinement for KSTAR With n=1 Resonant Magnetic Field Perturbation”, Nucl. Fusion 62, 026043 (2022).
[30] LOGAN, N. et al., “Improved Pedestal Performance Utilizing 3D Fields and Localized Electron Cyclotron Current Drive”, 29th IAEA Fusion Energy Conference (Proc. Int. Conf. London, UK, 2023), IAEA, Vienna (2023)
[31] ABRAMS, T., “Unravelling the Physics of Tungsten Sourcing and Leakage from a Slot Divertor Configuration on DIII-D”, 29th IAEA Fusion Energy Conference (Proc. Int. Conf. London, UK, 2023), IAEA, Vienna (2023)

[32] ABRAMS, T., et al., "Design and Physics Basis for the Upcoming DIII-D SAS-VW Campaign to Quantify Tungsten Leakage and Transport in a New Slot Divertor Geometry", Physica Scripta, 96, 124073 (2021).
[33] CHEN, X., "Recent Progress of the Reactor-Relevant Intrinsically ELM-Stable Quiescent H-Mode on the DIII-D Tokamak", 29th IAEA Fusion Energy Conference (Proc. Int. Conf. London, UK, 2023), IAEA, Vienna (2023)
[34] CHEN, X., et al. "Expanding the Parameter Space off the Wide-Pedestal QH-Mode Towards ITER Conditions", Nucl. Fusion, 60, 092006 (2020).
[35] HOUSHMANDYAR, S., et al., "Explaining the Lack of Power Degradation of Energy Confinement in Wide Pedestal Quiescent H-Modes Via Transport Modelling", Nucl. Fusion, 62, 056024 (2022).
[36] LI, Z., et al., "Numerical Modeling of Pedestal Stability and Broadband Turbulence of Wide-Pedestal QH-Mode Plasmas on DIII-D", Nucl. Fusion 62, 076033 (2022).
[37] ERNST, D. et al., "Broadening of the Divertor Heat Flux Profile in High Confinement Tokamak Fusion Plasmas with Edge Pedestals Limited by Turbulence", submitted to Phys. Rev. Lett., 2023.
[38] LI, Z., et al., "How Turbulence Spreading Improves Power Handling in Quiescent High Confinement Fusion Plasmas", submitted to Nature Communications
[39] SORBUM, B. et al., "ARC: A Compact, High-Field, Fusion Nuclear Science Facility and Demonstration Power Plant With Demountable Magnets", Fusion Eng. And Design, 100, 378 (2015).
[40] TURCO, F. "First Tungsten Radiation Studies and Non-Linear Oscillations in DIII-D's ITER Baseline Demonstration Discharges", 29th IAEA Fusion Energy Conference (Proc. Int. Conf. London, UK, 2023), IAEA, Vienna (2023)
[41] HANSON, J., "Variable-Spectrum Mode Control of High Poloidal Beta Discharges", 29th IAEA Fusion Energy Conference (Proc. Int. Conf. London, UK, 2023), IAEA, Vienna (2023)
[42] HUANG, J., "Sustainment of High q_{min}, High β_N Plasmas on DIII-D Towards Steady-State Advanced Tokamak Fusion, 29th IAEA Fusion Energy Conference (Proc. Int. Conf. London, UK, 2023), IAEA, Vienna (2023)
[43] BERNARD, L. et al., "GATO: An MHD Stability Code for Axisymmetric Plasmas With Internal Separatrices", Comp. Phys. Comm., 24, 377 (1981).
[44] CHEN, X. et al., "Doubling Off-Axis Electron Cyclotron Current Drive Efficiency Via Velocity Space Engineering", Nucl. Fusion, 62, 054001 (2022).
[45] VAN COMPERNOLLE, B. et al., "The High-Power Helicon Program at DIII-D: Gearing Up For First Experiments", Nucl. Fusion, 61, 116034 (2021).
[46] WUKITCH, S., "Development of DIII-D high Field Side Lower Hybrid Current Drive Launcher", 29th IAEA Fusion Energy Conference (Proc. Int. Conf. London, UK, 2023), IAEA, Vienna (2023)
[47] THOME, K., "Assessment of Negative Triangularity as a Reactor Scenario in DIII-D", 29th IAEA Fusion Energy Conference (Proc. Int. Conf. London, UK, 2023), IAEA, Vienna (2023)
[48] CAMENEN, Y. et al., "Impact of Plasma Triangularity and Collisionality On Electron Heat Transport in TCV L-Mode Plasmas", Nucl. Fusion, 47, 510 (2007).
[49] AUSTIN, M., et al., "Achievement of Reactor-Relevant Performance in Negative Triangularity Shape in the DIII-D Tokamak", Phys. Rev. Lett., 122, 115001 (2019).
[50] NELSON, A. et al., "Robust L-Mode Edge Behaviour in High Performance Negative Triangularity Plasmas: From Experiments to Reactors", 29th IAEA Fusion Energy Conference (Proc. Int. Conf. London, UK, 2023), IAEA, Vienna (2023)
[51] SAARELMA, S. et al., "Ballooning Instability Preventing the H-Mode Access in Plasmas With Negative Triangularity Shape on the DIII-D Tokamak", Plasma Physics And Controlled Fusion, 63, 105006 (2021).
[52] SCOTTI, F. et al., "Characterization of Scrape-Off Layer Radial Transport and Access to Detached Divertor Conditions in Discharges With Negative Triangularity Shaping in the DIII-D Tokamak", submitted to Nucl. Fusion
[53] JAERVINEN, A. et al., "ExB Flux Driven Detachment Bifurcation in the DIII-D Tokamak", Phys. Rev. Lett., 121, 075001, (2018).
[54] KIKUCHI, M. et al., "L-Mode-Edge Negative Triangularity Tokamak Reactor", Nucl. Fusion, 59, 056017 (2019).
[55] IZZO, V., "Simulations of Shell Pellet Injection Strategies for ITER-Scale Tokamaks", Plasma Physics and Controlled Fusion, 65, 095007 (2023).
[56] IZZO, V., "Runaway Electron Prevention by a Passive 3D Coil in Disruption Simulations of the SPARC and DIII-D Tokamaks", 29th IAEA Fusion Energy Conference (Proc. Int. Conf. London, UK, 2023), IAEA, Vienna (2023)

2023 AUTHOR LIST

User Last Name	User First Name	Home Institution Name
Abbate	Joseph	Princeton Plasma Physics Laboratory
Abe	Shota	Princeton Plasma Physics Laboratory
Abrams	Tyler	General Atomics
Adebayo-ige	Promise	University of Tennessee, Knoxville
Agabian	Susan	Massachusetts Institute of Technology
Ahmed	Sajidah	UiT The Arctic University of Norway
Aiba	Nobuyuki	QST
Akcay	Cihan	General Atomics
Akiyama	Tsuyoshi	General Atomics
Albosta	Ryan	University of Wisconsin
Aleynikov	Pavel	Max-Planck Institute for Plasma Physics
Allen	Steve	Lawrence Livermore National Laboratory
Anand	Himank	General Atomics
Anderson	James	General Atomics
Andrew	Yasmin	Imperial College London
Ashburn	Michael	University of Tennessee, Knoxville
Ashourvan	Arash	General Atomics
Austin	Max	University of Texas, Austin
Avdeeva	Galina	General Atomics
Ayala	David	General Atomics
Ayub	Muhammad Saad	General Atomics
Bagdy	Esteban	General Atomics
Banerjee	Santanu	Princeton Plasma Physics Laboratory
Barada	Kshitish Kumar	University of California, Los Angeles
Bardoczi	Laszlo	General Atomics
Bardsley	Oliver	UKAEA
Barr	Jayson	General Atomics
Bass	Eric	University of California, San Diego
Battey	Alexander	Columbia University
Bayler	Zachary	University of Denver
Baylor	Larry	Oak Ridge National Lab
Bechtel	Torrin	Oak Ridge Associated Universities
Beidler	Matthew	Oak Ridge National Lab
Belli	Emily	General Atomics
Benedett	Thomas	University of California, Los Angeles
Bergstrom	Zachary	General Atomics
Berkel	Matthijs	Eindhoven Unversity of Technology
Bernard	Tess	General Atomics
Bertelli	Nicola	Princeton Plasma Physics Laboratory
Bielajew	Rachel	Massachusetts Institute of Technology
Bodner	Grant	General Atomics
Boedo	Jose	University of California, San Diego
Boivin	Rejean	General Atomics
Bolzonella	Tommaso	Consorzio RFX

Bonoli	Paul	Massachusetts Institute of Technology
Bortolon	Alessandro	Princeton Plasma Physics Laboratory
Bose	Sayak	Princeton Plasma Physics Laboratory
Boyer	Mark	Princeton Plasma Physics Laboratory
Boyes	William	Columbia University
Bradley	Larry	University of California, Los Angeles
Brambila	Rigo	General Atomics
Braun	Anson	Columbia University
Brennan	Dylan	Princeton University
Bringuier	Stefan	General Atomics
Brodsky	Luda	General Atomics
Brookman	Michael	Princeton Plasma Physics Laboratory
Brooks	Jeffrey	Purdue University
Brower	David	University of California, Los Angeles
Brown	William	Princeton Plasma Physics Laboratory
Buck	Joseph	Brigham Young University
Buczek	Sean	General Atomics
Burgess	Daniel	Columbia University
Burke	Marcus	Lawrence Livermore National Laboratory
Burrell	Keith	General Atomics
Butt	Jalal-ud-din	Columbia University
Buttery	Richard	General Atomics
Bykov	Igor	General Atomics
Byrne	Patrick	General Atomics
Cacheris	Alec	University of Tennessee, Knoxville
Callahan	Kyle	University of California, Los Angeles
Callen	James	University of Wisconsin
Campbell	Dan	NVIDIA
Candy	Jeffrey	General Atomics
Canik	John	Oak Ridge National Lab
Cappelli	Luca	CEA Cadarache
Carlstrom	Thomas	General Atomics
Carr	Richard	General Atomics
Carrig	Will	General Atomics
Carter	Blake	General Atomics Temp
Carter	Troy	University of California, Los Angeles
Carvalho	Ivo	General Atomics
Cary	William	General Atomics
Casali	Livia	University of Tennessee, Knoxville
Ceelen	Lennard	Eindhoven Unversity of Technology
Cengher	Mirela	General Atomics
Cha	Matthew	General Atomics
Chaban	Ryan	College of William and Mary
Chan	Vincent	Self-Employed
Chapman	Brett	University of Wisconsin
Char	Ian	Carnegie Mellon University
Chen	Jiale	ASIPP
Chen	Ran	ASIPP

Chen	Jie	University of California, Los Angeles
Chen	Xi	General Atomics
Chen	Yvonne	University of California, San Diego
Chiriboga	Javier	College of William and Mary
Cho	Elizabeth	General Atomics
Choi	Gyungjin	Seoul National University
Choi	Wilkie	General Atomics
Choudhury	Hari	Columbia University
Chowdhury	Satyajit	University of California, Los Angeles
Chrystal	Colin	General Atomics
Chung	Youngseog	Carnegie Mellon University
Churchill	Randy	Princeton Plasma Physics Laboratory
Clark	Randall	General Atomics
Clement	Mitchell	Princeton Plasma Physics Laboratory
Coburn	Jonathan	Sandia National Lab
Coda	Stefano	EPFL
Coffee	Ryan	SLAC
Collins	Cami	Oak Ridge National Lab
Colmenares-Fernandez	Juan	General Atomics
Conlin	William	Princeton University
Coon	Robert	General Atomics
Cote	Tyler	Oak Ridge Associated Universities
Creely	Alexander	Commonwealth Fusion Systems
Crocker	Neal	University of California, Los Angeles
Crowe	Christopher	General Atomics
Crowley	Brendan	General Atomics
Crowley	Thomas	Xantho Technologies, LLC
Curie	Max	University of Texas, Austin
Curreli	Davide	University of Illinois, Urbana-Champaign
Dal Molin	Andrea	Istituto di Fisica del Plasma CNR-EURATOM
Damba	Julius	University of California, Los Angeles
Dart	Eli	Lawrence Berkeley National Laboratory
Dautt-Silva	Alicia	General Atomics
Davda	Kirtan	University of Tennessee, Knoxville
De	Aritra	Oak Ridge Associated Universities
de Boucaud	Nikolai	General Atomics
de Jong	Yannick	Eindhoven Unversity of Technology
DE VRIES	PETER	ITER Organization
de-Villeroche	Armand	ENS Paris Saclay
DeGrandchamp	Genevieve	University of California, Irvine
deGrassie	John	General Atomics
Demers	Diane	Xantho Technologies, LLC
Denk	Severin	Massachusetts Institute of Technology
DeShazer	Earl	General Atomics
Di Genova	Stefano	CEA Cadarache
Diallo	Ahmed	Princeton Plasma Physics Laboratory
Dimits	Andris	Lawrence Livermore National Laboratory

Ding	Rui	ASIPP
Ding	Siye	Oak Ridge Associated Universities
Donovan	David	University of Tennessee, Knoxville
Du	Xiaodi	General Atomics
Dunsmore	James	Imperial College London
Dupuy	Alex	General Atomics
Duran	Jonah	University of Tennessee, Knoxville
Dvorak	Andrew	Oak Ridge National Lab
Effenberg	Florian	Princeton Plasma Physics Laboratory
Eidietis	Nicholas	General Atomics
Elder	David	University of Toronto
Eldon	David	General Atomics
Elsey	Tyler	General Atomics
Ennis	David	Auburn University
Erickson	Keith	Princeton Plasma Physics Laboratory
Ernst	Darin	Massachusetts Institute of Technology
Fajardo	Max	Portland State University
Farre-Kaga	Hiro-Josep	Imperial College London
Fenstermacher	Max	Lawrence Livermore National Laboratory
Ferraro	Nathaniel	Princeton Plasma Physics Laboratory
Ferron	John	General Atomics
Feyrer	Abigail	University of Michigan
Fimognari	Peter	Xantho Technologies, LLC
Finden	Ryan	General Atomics
Finkenthal	Daniel	Palomar Scientific Instruments, Inc
Fitzpatrick	Richard	University of Texas, Austin
Flanagan	Sean	General Atomics
Ford	Brent	University of Wisconsin
Fox	William	Princeton Plasma Physics Laboratory
Freiberger	Samuel	Columbia University
Fu	Lanke	Princeton Plasma Physics Laboratory
Gage	Kenneth	University of California, Irvine
Gajaraj	Vaisnav	Princeton Plasma Physics Laboratory
Garcia	Ivan	Massachusetts Institute of Technology
Garcia	Fernando	General Atomics
Garcia	Alvin	University of California, Irvine
Garcia Munoz	Manuel	University of Seville
Garnier	Darren	Massachusetts Institute of Technology
Garofalo	Andrea	General Atomics
Gattuso	Anthony	General Atomics
Geiger	Benedikt	University of Wisconsin
Gentle	Kenneth	University of Texas, Austin
Ghai	Yashika	Oak Ridge National Lab
Gill	Kevin	University of Wisconsin
Glass	Fenton	General Atomics
Gohil	Punit	General Atomics
Gong	Xianzu	ASIPP
Gonzalez-Martin	Javier	University of California, Irvine

Gorelov	Yuri	General Atomics
Graber	Vincent	Lehigh University
Granetz	Robert	Massachusetts Institute of Technology
Gray	Clayton	General Atomics
Greenfield	Charles	General Atomics
Grierson	Brian	General Atomics
Groebner	Richard	General Atomics
Grosnickle	William (Bill)	General Atomics
Groth	Mathias	Aalto University
Gu	Shuai	Oak Ridge Associated Universities
Guo	Houyang	General Atomics
Guterl	Jerome	General Atomics
Guttenfelder	Walter	Princeton Plasma Physics Laboratory
Hager	Robert	Princeton Plasma Physics Laboratory
Hahn	Sang-hee	Korea Institute of Fusion Energy
Halfmoon	Michael	University of Texas, Austin
Hall	Joseph	Brown University
Hall-Chen	Valerian	Institute of High Performance Computing
Halpern	Federico	General Atomics
Hammett	Greg	Princeton Plasma Physics Laboratory
Han	Xiang	University of Wisconsin
Hansen	Chris	University of Washington
Hansen	Erik	University of California, Irvine
Hanson	Jeremy	Columbia University
Hanson	Michael	University of California, San Diego
Harris	Ashley	General Atomics
Harvey	Robert	CompX
Haskey	Shaun	Princeton Plasma Physics Laboratory
Hatch	David	Fusion Energy Associates
Hayashi	Wataru	University of California, Irvine
Hayes	Alyssa	University of Tennessee, Knoxville
Heidbrink	William	University of California, Irvine
Herfindal	Jeffrey	Oak Ridge National Lab
Hicok	Joshua	General Atomics
Hinson	Edward	University of Wisconsin
Hisakado	Tomu	General Atomics
Holcomb	Christopher	Lawrence Livermore National Laboratory
Holland	Christopher	University of California, San Diego
Holland	Leo	General Atomics
Hollmann	Eric	University of California, San Diego
Holm	Andreas	Aalto University
Holmes	Ian	General Atomics
Holtrop	Kurt	General Atomics
Hong	Rongjie	University of California, Los Angeles
Hood	Ryan	Sandia National Lab
Horvath	Laszlo	UKAEA
Houshmandyar	Saeid	General Atomics

Howard	Nathan	Massachusetts Institute of Technology
Howell	Eric	Tech-X Corporation
Hu	Wenhui	ASIPP
Hu	Yunchan	ASIPP
Hu	Qiming	Princeton Plasma Physics Laboratory
Huang	Yao	Chinese Academy of Sciences
Huang	Juan	ASIPP
Huang	Aaron	University of California, Santa Barbara
Hubbard	Amanda	Massachusetts Institute of Technology
Hughes	Jerry	Massachusetts Institute of Technology
Humphreys	David	General Atomics
Hurtado	Joel	San Diego Mesa College
Hyatt	Alan	General Atomics
Imada	Koki	University of York
Izzo	Valerie	Fiat Lux
Jalalvand	Azarakhsh	Ghent University
Jardin	Stephen	Princeton Plasma Physics Laboratory
Jarvinen	Aaro	VTT Technical Research Centre
Jeon	Young-Mu	Korea Institute of Fusion Energy
Ji	Hantao	Princeton University
Jian	Xiang	University of California, San Diego
Jian	Laura	University of California, San Diego
Jiang	Yanzheng	General Atomics
Johnson	Curtis	Oak Ridge National Lab
Johnson	Jamal	Massachusetts Institute of Technology
Jones	Michael	Brigham Young University
Joung	Semin	University of Wisconsin
Jouzdani	Pejman	General Atomics
Jung	Euichan	Princeton University
Kallenberg	Evan	General Atomics
Kalling	Richard	Kalling Software
Kaplan	David	General Atomics
Kaptanoglu	Alan	University of Maryland
Kellman	Daniel	General Atomics
Kennedy	James	University of Florida
Khabanov	Filipp	University of Wisconsin
Kim	Jayhyun	Korea Institute of Fusion Energy
Kim	Hyunseok	Korea Institute of Fusion Energy
Kim	Eun-jin	Coventry University
Kim	SangKyeun	Princeton University
Kim	Kyungjin	Oak Ridge National Lab
Kim	Charlson	SLS2 Consulting
Kim	Tierney	Point Loma Nazarene University
King	Jacob	Tech-X Corporation
Kinsey	Jon	CompX
Kirk	Andrew	CCFE
Klasing	Daniel	University of Tennessee, Knoxville
Kleiner	Andreas	Princeton Plasma Physics Laboratory

Knolker	Matthias	General Atomics
Kochan	Martin	CCFE
Koel	Bruce	Princeton University
Koenders	Jesse	Eindhoven Unversity of Technology
Koepke	Mark	West Virginia University
Kolasinski	Robert	Sandia National Lab
Kolemen	Egemen	Princeton Plasma Physics Laboratory
Kostadinova	Evdokiya	Auburn University
Kostuk	Mark	General Atomics
Kramer	Gerrit	Princeton Plasma Physics Laboratory
Kube	Ralph	Princeton Plasma Physics Laboratory
Kumar	Neeraj	University of Colorado, Boulder
La Haye	Robert	Retired from General Atomics
Laggner	Florian	Princeton Plasma Physics Laboratory
Lahban	Courage	Princeton Plasma Physics Laboratory
Lan	Heng	ASIPP
Landry	Rich	Massachusetts Institute of Technology
Lantsov	Roman	University of California, Los Angeles
Lao	Lang	General Atomics
Lasnier	Charles	Lawrence Livermore National Laboratory
Lau	Cornwall	Oak Ridge National Lab
Leccacorvi	Rick	Massachusetts Institute of Technology
Leddy	Jarrod	Tech-X Corporation
Lee	Myungwon	National Fusion Research Institute
Lee	Seungsup	University of Tennessee, Knoxville
Lee	KuanWei	University of Tennessee, Knoxville
Lee	Richard	General Atomics
Lehnen	Michael	ITER Organization
Leonard	Anthony	General Atomics
Leppink	Evan	Massachusetts Institute of Technology
LeSher	Michael	General Atomics
Lestz	Jeffrey	University of California, Irvine
Leuer	James	General Atomics
Leuthold	Nils	Oak Ridge Associated Universities
Li	Guoqiang	ASIPP
Li	Xiaoliang	ASIPP
Li	Yongliang	ASIPP
Li	Li	Donghua University
Li	Nami	Lawrence Livermore National Laboratory
Li	Zeyu	Oak Ridge Associated Universities
Lin	Daniel	General Atomics
Lin	Zihan	Princeton University
Lin	Zhihong	University of California, Irvine
Lin	Yijun	Massachusetts Institute of Technology
Linsenmayer	Erik	General Atomics
Liu	Jianbin	ASIPP
Liu	Deyong	General Atomics

Liu	Dingyun	Princeton University
Liu	Chang	Princeton Plasma Physics Laboratory
Liu	Zefang	Georgia Tech
Liu	Yueqiang	General Atomics
Liu	Caizhen	General Atomics
Loarte-Prieto	Alberto	ITER Organization
Loch	Stuart	Auburn University
LoDestro	Lynda	Lawrence Livermore National Laboratory
Logan	Nikolas	Lawrence Livermore National Laboratory
Lohr	John	General Atomics
Lore	Jeremy	Oak Ridge National Lab
Losada Rodriguez	Ulises	Auburn University
Loughran	Jarred	College of William and Mary
Lowell	Maya	University of California, Los Angeles
Luce	Timothy	ITER Organization
Luhmann	Neville	University of California, Davis
Lunia	Priyansh	Columbia University
Lunsford	Robert	Princeton Plasma Physics Laboratory
Lupin-Jimenez	Leonard	Princeton Plasma Physics Laboratory
Lvovskiy	Andrey	General Atomics
Lyons	Brendan	General Atomics
Ma	Xinxing	General Atomics
MacDonald	James	General Atomics
Macwan	Tanmay Martinbhai	University of California, Los Angeles
Maingi	Rajesh	Princeton Plasma Physics Laboratory
Major	Maximillian	University of Wisconsin
Malhotra	Lakshya	University of Wisconsin
Margo	Martin	General Atomics
Marini	Claudio	University of California, San Diego
Marinoni	Alessandro	Massachusetts Institute of Technology
Maris	Andrew	Massachusetts Institute of Technology
Martin	Elijah	Oak Ridge National Lab
Mateja	Jeremy	University of Tennessee, Knoxville
Mattes	Ray	University of Tennessee, Knoxville
Maurizio	Roberto	Oak Ridge Associated Universities
Mauzey	David	Princeton Plasma Physics Laboratory
McAllister	Levi	General Atomics
McArdle	Graham	CCFE
McClenaghan	Joseph	General Atomics
McCollam	Karsten	University of Wisconsin
McKee	George	University of Wisconsin
McLaughlin	Kevin	General Atomics
McLean	Adam	Lawrence Livermore National Laboratory
Mehta	Viraj	Carnegie Mellon University
Meier	Eric	Zap Energy Inc.
Meitner	Steve	Oak Ridge National Lab
Menard	Jonathan	Princeton Plasma Physics Laboratory

Meneghini	Orso	General Atomics
Merlo	Gabriele	University of Texas, Austin
Messer	Seth	University of Tennessee, Knoxville
Meyer	William	Lawrence Livermore National Laboratory
Michael	Clive	University of California, Los Angeles
Miller	David	General Atomics
Miller	Marco	Massachusetts Institute of Technology
Mitchell	Joshua	UKAEA
Mitra	Elena	Princeton University
Moeller	Charles	General Atomics
Mohamed	Mohamed	Massachusetts Institute of Technology
Molesworth	Steven	University of California, San Diego
Montes	Kevin	Massachusetts Institute of Technology
Mordijck	Saskia	The College of William and Mary
Morosohk	Shira	Lehigh University
Moser	Auna	General Atomics
Mueller	Dennis	Princeton Plasma Physics Laboratory
Munaretto	Stefano	Princeton Plasma Physics Laboratory
Murphy	Christopher	General Atomics
Muscatello	Christopher	General Atomics
Myers	Rachel	University of Wisconsin
Nagy	Alexander	Princeton Plasma Physics Laboratory
Nath	Dhyanjyoti	Rensselaer Polytechnic Institute
Navarro	Marcos	University of Wisconsin
Nazikian	Raffi	General Atomics
Neiser	Tom	General Atomics
Nelson	Andrew	Columbia University
Nesbet	Perry	General Atomics
Nespoli	Federico	Princeton Plasma Physics Laboratory
Nguyen	Paul	General Atomics
Nguyen	Duy	General Atomics
Nguyen	Randy	General Atomics
Nichols	Jacob	Oak Ridge National Lab
Nocente	Massimo	Universita di Milano-Bicocca
Nuckols	Lauren	Oak Ridge National Lab
Nygren	Richard	Sandia National Lab
Odstrcil	Tomas	General Atomics
Okabayashi	Michio	Princeton Plasma Physics Laboratory
Olofsson	Erik	General Atomics
Orlov	Dmitriy	University of California, San Diego
Orozco	David	General Atomics
Osborne	Nicholas	University of Liverpool
Osborne	Thomas	General Atomics
OShea	Finn	SLAC
Pace	David	General Atomics
Packard	Drew	General Atomics
Pajares Martinez	Andres	General Atomics

Pakosta	Christopher	General Atomics
pan	chengkang	ASIPP
Pandya	Mihir	University of Wisconsin
Panici	Dario	Princeton University
Pankin	Alexei	Princeton Plasma Physics Laboratory
Park	Young-Seok	Columbia University
Park	Jin Myung	Oak Ridge National Lab
Park	Jong-Kyu	Princeton Plasma Physics Laboratory
Parker	Carl	General Atomics
Parker	Scott	University of Colorado, Boulder
Parks	Paul	General Atomics
Parsons	Matthew	The Pennsylvania State University
Paruchuri	Sai-Tej	Lehigh University
Paz-Soldan	Carlos	Columbia University
Pederson	Troy	General Atomics
Peebles	William	University of California, Los Angeles
Penaflor	Benjamin	General Atomics
Perez	Elizabeth	University of Wisconsin
Periasamy	Lavanya	General Atomics
Perillo	Renato	University of California, San Diego
Petty	Clinton (Craig)	General Atomics
Pharr	Matthew	Columbia University
Pierce	Don	General Atomics
Pierren	Christopher	University of Wisconsin
Pierson	Sam	Massachusetts Institute of Technology
Pigarov	Alexander	CompX
Pigatto	Leonardo	Consorzio RFX
Piglowski	David	General Atomics
Pinches	Simon	ITER Organization
Pinsker	Robert	General Atomics
Pitts	Richard	ITER Organization
Pizzo	Jonathan	University of Wisconsin
Podesta	Mario	Princeton Plasma Physics Laboratory
Popovic	Zana	Oak Ridge Associated Universities
Porkolab	Miklos	Massachusetts Institute of Technology
Pratt	Quinn	University of California, Los Angeles
Prechel	Garrett	University of California, Irvine
Pusztai	Istvan	Chalmers University of Technology (Sweden)
Puthan-Naduvakkate	Pranav-Suresh	Oak Ridge Associated Universities
Qian	Jinping	ASIPP
Qin	Xijie	University of Wisconsin
Ra	OokJoo	Ulsan National Institute of Science and Technology
Raines	Taylor	Princeton Plasma Physics Laboratory
Rakers	Kole	University of Wisconsin
Rath	Katharina	Max-Planck Institute for Plasma Physics
Rauch	Joseph	General Atomics
Rea	Cristina	Massachusetts Institute of Technology

Reed	Ramon	Princeton Plasma Physics Laboratory
Reiman	Allan	Princeton Plasma Physics Laboratory
Reinke	Matthew	Commonwealth Fusion Systems
Reksoatmodjo	Richard	College of William and Mary
Ren	Qilong	ASIPP
Ren	Jun	University of Tennessee, Knoxville
Ren	Yang	Princeton Plasma Physics Laboratory
Rensink	Marvin	Lawrence Livermore National Laboratory
Rhodes	Terry	University of California, Los Angeles
Richner	Nathan	Oak Ridge Associated Universities
Ridzon	James	Massachusetts Institute of Technology
Riggs	Gregory	West Virginia University
Riquezes	Juan	Columbia University
Rodriguez Fernandez	Pablo	Massachusetts Institute of Technology
Rognlien	Thomas	Lawrence Livermore National Laboratory
Ronchi	Gilson	Oak Ridge National Lab
Rondini	Lucia	Columbia University
Rosati	Ron	Massachusetts Institute of Technology
Rosenthal	Aaron	Massachusetts Institute of Technology
Ross	Michael	General Atomics
Rost	Jon (Chris)	Massachusetts Institute of Technology
Rothstein	Andrew	Princeton University
Roveto	Jonathan	Georgia Tech
Ruane	James	General Atomics
Rudakov	Dmitry	University of California, San Diego
Rupani	Rushabh	General Atomics
Rutherford	Grant	Massachusetts Institute of Technology
Sabbagh	Steven	Columbia University
Sachdev	Jai	Princeton Plasma Physics Laboratory
Sadeghi	Nima	University of California, Los Angeles
Salmi	Antti	VTT Technical Research Centre
Salvador	Felipe	University of Sao Paulo, Insitute of Physics
Sammuli	Brian	General Atomics
Samuell	Cameron	Lawrence Livermore National Laboratory
Sandorfi	Andrew	Jefferson Lab
Sang	Chaofeng	Dalian University of Technology
Santa	Dylan	ORISE
Sarff	John	University of Wisconsin
Sauter	Olivier	EPFL
Savelli	Henry	Massachusetts Institute of Technology
Schaefer	Carolyn	University of Wisconsin
Schamis	Hanna	The Pennsylvania State University
Schellpfeffer	Jacob	University of Wisconsin
Schissel	David	General Atomics
Schmitz	Lothar	University of California, Los Angeles
Schmitz	Oliver	University of Wisconsin
Schroeder	Paul	General Atomics

Schultz	Karl	General Atomics
Schuster	Eugenio	Lehigh University
Sciortino	Francesco	Max-Planck Institute for Plasma Physics
Scotti	Filippo	Lawrence Livermore National Laboratory
Scoville	John	General Atomics
Seltzman	Andrew	Massachusetts Institute of Technology
Seo	Jaemin	Princeton University
Serrano	Jesus	University of California, Los Angeles
Sfiligoi	Igor	University of California, San Diego
Shafer	Morgan	Oak Ridge National Lab
Shapov	Ron	General Atomics
Shen	Hanhong	General Atomics
Shi	Nan	General Atomics
Shiraki	Daisuke	Oak Ridge National Lab
Short	Brendan	General Atomics
Shousha	Ricardo	Princeton University
Si	Hang	ASIPP
Sierra	Carlos	University of Florida
Sinclair	Gregory	General Atomics
Sinha	Priyanjana	Princeton Plasma Physics Laboratory
Sips	George	General Atomics
Skinner	Charles	Princeton Plasma Physics Laboratory
Slendebroek	Tim	Oak Ridge Associated Universities
Slief	Jelle	Eindhoven Unversity of Technology
Smirnov	Roman	University of California, San Diego
Smith	Sterling	General Atomics
Smith	David	University of Wisconsin
Snoep	Garud	Eindhoven Unversity of Technology
Snyder	Philip	Oak Ridge National Lab
Solomon	Wayne	General Atomics
Song	Xiao	Lehigh University
Sontag	Aaron	University of Wisconsin
Soukhanovskii	Vsevolod	Lawrence Livermore National Laboratory
Spong	Donald	Oak Ridge National Lab
Squire	Jared	General Atomics
Staebler	Gary	General Atomics
Stagner	Luke	General Atomics
Stange	Torsten	Max-Planck Institute for Plasma Physics
Stangeby	Peter	University of Toronto
Starling	Elizabeth	Oak Ridge Associated Universities
Stewart	Samuel	University of Wisconsin
Stoltzfus-Dueck	Timothy	Princeton Plasma Physics Laboratory
Storment	Stephen	University of California, Los Angeles
Strait	Edward (Ted)	General Atomics
Su	David	General Atomics
Sugiyama	Linda	Massachusetts Institute of Technology
Sun	Pengjun	ASIPP
Sun	Yanxu	ASIPP

Sun	Youwen	ASIPP
Sun	Xuan	Oak Ridge Associated Universities
Sung	Choongki	KAIST
Suttrop	Wolfgang	Max-Planck Institute for Plasma Physics
Suzuki	Yasuhiro	Hiroshima University
Sweeney	Ryan	Massachusetts Institute of Technology
Taczak	Benjamin	Bowdoin College
Takemura	Yuki	National Institute for Fusion Science, Japan
Tang	Shawn Wenjie	University of California, San Diego
Tang	Shawn	Oak Ridge Associated Universities
Tang	William	Princeton University
Tardini	Giovanni	Max-Planck Institute for Plasma Physics
Taussig	Doug	General Atomics
Teixeira	Kyle	General Atomics
Thackston	Kyle	General Atomics
Thomas	Dan	General Atomics
Thome	Kathreen	General Atomics
Tinguely	Roy	Massachusetts Institute of Technology
Tobin	Matt	Columbia University
Tooker	Joseph	General Atomics
Torrezan de Sousa	Antonio	General Atomics
Traverso	Peter	Auburn University
Trevisan	Gregorio Luigi	Self-Employed
Trier	Elisee	UKAEA
Truong	Dinh	Sandia National Lab
Tsui	Cedric	University of California, San Diego
Turco	Francesca	Columbia University
Turnbull	Alan	General Atomics
Turner	Lucas	University of Tennessee, Knoxville
Unterberg	Ezekial	Oak Ridge National Lab
Van Compernolle	Bart	General Atomics
van Kampen	Ricky	Eindhoven Unversity of Technology
Van Zeeland	Michael	General Atomics
Victor	Brian	Lawrence Livermore National Laboratory
Vieira	Rui	Massachusetts Institute of Technology
Viezzer	Eleonora	University of Seville
Vincena	Stephen	University of California, Los Angeles
Vollmer	Devin	General Atomics
Wai	Josiah	Princeton University
Walker	Michael	General Atomics
Waltz	Ronald	General Atomics
Wampler	William	Sandia National Lab
Wang	Liang	ASIPP
Wang	Yifeng	ASIPP
Wang	Huiqian	General Atomics
Wang	Zibo	Lehigh University
Wang	Guiding	University of California, Los Angeles

Wang	Allen	Massachusetts Institute of Technology
Watkins	Jonathan	Sandia National Lab
Watkins	Matthias	General Atomics
Watts	Thomas	University of Texas, Austin
Webber	Logan	General Atomics
Weber	Kennith	Princeton Plasma Physics Laboratory
Wehner	William	General Atomics
Wei	Xishuo	University of California, Irvine
Weisberg	David	General Atomics
Welander	Anders	General Atomics
Welsh	Austin	University of Tennessee, Knoxville
White	Andrew	Auburn University
Wilcox	Robert	Oak Ridge National Lab
Wilkie	George	Princeton Plasma Physics Laboratory
Wilks	Theresa	Massachusetts Institute of Technology
Willensdorfer	Matthias	Max-Planck Institute for Plasma Physics
Wilson	Haley	Columbia University
Wingen	Andreas	Oak Ridge National Lab
Wu	Muquan	ASIPP
Wu	Donggui	ASIPP
Wukitch	Stephen	Massachusetts Institute of Technology
Xia	Jamie	University of Washington
Xie	Ruifeng	University of Texas, Austin
Xing	Zichuan	General Atomics
Xu	Guoliang	ASIPP
xu	xueqiao	Lawrence Livermore National Laboratory
Yan	Zheng	University of Wisconsin
Yang	Xu	Dalian University of Technology
Yang	Lixing	Lehigh University
Yang	Seong-moo	Princeton Plasma Physics Laboratory
Yang	Jeong-hun	Princeton Plasma Physics Laboratory
Yoo	Mingoo	General Atomics
YU	GUANYING	University of California, Davis
Yu	Jonathan	General Atomics
Zalzali	Amani	Oak Ridge Associated Universities
Zamengo	Andrea	General Atomics
Zamkovska	Veronika	Columbia University
Zamperini	Shawn	General Atomics
Zarrabi	Kian	General Atomics
Zeger	Emi	University of California, Los Angeles
Zeller	Kurt	General Atomics
Zeng	Lei	University of California, Los Angeles
Zhang	Xinjun	ASIPP
Zhang	Jie	ASIPP
Zhang	Bin	ASIPP
Zhang	Jiayuan	ASIPP
Zhao	Bingzhe	University of Texas, Austin
Zhao	Chen	General Atomics

Zheng	Yuan	University of California, Davis
Zhu	Yilun	University of California, Davis
Zhu	Jinxiang	Massachusetts Institute of Technology
Ziegel	Joseph	University of Texas, Austin
Zimmerman	Jeffrey	University of Wisconsin
Zuniga	Christian	General Atomics